Separating Energetic Internal Gravity Waves and Small-Scale Frontal Dynamics

Hector S. Torres, Patrice Klein, Eric d'Asaro, Jinbo Wang, Andrew F. Thompson, Lia Siegelman, Dimitris Menemenlis, Ernesto Rodriguez, Alexander Wineteer, Dragana Perkovic-Martin

Geophysical Research Letters

RESEARCH LETTER
10.1029/2021GL096249

Key Points:

- Vertical transport due to convergence at surface fronts is obscured by internal gravity waves in a model of the California Current
- Contamination by low-mode internal waves can be reduced by filtering large vertical scales
- A simple filtering algorithm can effectively remove internal waves with little impact on frontal dynamics in the model

Supporting Information:

Supporting Information may be found in the online version of this article.

Correspondence to:

H. S. Torres,
Hector.Torres.Gutierrez@jpl.nasa.gov

Citation:

Torres, H. S., Klein, P., D'Asaro, E., Wang, J., Thompson, A. F., Siegelman, L., et al. (2022). Separating energetic internal gravity waves and small-scale frontal dynamics. *Geophysical Research Letters*, *49*, e2021GL096249. https://doi.org/10.1029/2021GL096249

Received 30 SEP 2021
Accepted 18 FEB 2022

Separating Energetic Internal Gravity Waves and Small-Scale Frontal Dynamics

Hector S. Torres[1], Patrice Klein[1,2,3], Eric D'Asaro[4], Jinbo Wang[1], Andrew F. Thompson[2], Lia Siegelman[5], Dimitris Menemenlis[1], Ernesto Rodriguez[1], Alexander Wineteer[1], and Dragana Perkovic-Martin[1]

[1]Jet Propulsion Laboratory, California Institute of Technology, Pasadena, CA, USA, [2]Environmental Science and Engineering, California Institute of Technology, Pasadena, CA, USA, [3]Laboratoire de Météorologie Dynamique, Ecole Normale Supérieure, CNRS, Paris, France, [4]Applied Physics Laboratory, University of Washington, Seattle, WA, USA, [5]Scripps Institution of Oceanography, UCSD, San Diego, CA, USA

Abstract Oceanic fronts with lateral scales less than 20 km are now known to be one of the major contributors to vertical heat fluxes in the global ocean, which highlights their potential impact on Earth's climate. However, frontal dynamics with time scales less than 1 day, whose contribution to vertical heat fluxes is thought to be significant, are obscured by energetic internal gravity waves (IGWs). In this study, we address this critical issue by separating IGWs and frontal dynamics using an approach based on their respective vertical scales of variability. Results using a numerical model with a horizontal grid spacing of 500 m confirm that it is possible to recover frontal dynamics at short time scales as well as associated intense vertical velocities and vertical heat fluxes. This opens up new possibilities for a more accurate estimation of the vertical exchanges of any tracers between the surface and the ocean interior.

Plain Language Summary Two classes of motions involving large vertical velocities are present in the upper ocean: Those associated with small-scale fronts (<20 km, also called submesoscale or SBM fronts) and those associated with internal gravity waves (IGWs). SBM fronts are known to explain most of the vertical transport of heat, nutrients, and major gases. IGWs do not transport tracers. Rather, small-scale IGWs are thought to lead to irreversible mixing through breaking. One issue that arises when analyzing in-situ observations and numerical simulations is how to discriminate between SBMs and IGWs when both classes of motions are energetic, such as in the California Current System. In this study, we show that SBM fronts and IGWs exhibit different vertical scales, which can be exploited to separate the two classes of motions. Our results confirm that filtering the contribution of large vertical scales to 3-dimensional velocity fields leads to an almost complete recovery of SBM frontal dynamics at short time scales. The significance of this separation is illustrated by the impact of short-time-scale, frontal-induced vertical velocity on vertical heat fluxes.

1. Introduction

In the last 15 years, numerical studies and field experiments have led to an important discovery. Frontal structures with lateral scales less than 20 km have a strong impact on the vertical transport of heat, nutrients, and important climatic gases between the ocean surface and interior (D'Asaro et al., 2011; Ferrari, 2011; Fox-Kemper et al., 2011; Klein et al., 2019; Su et al., 2018; Thompson et al., 2016). These small-scale fronts are usually in geostrophic or gradient-wind balance and are called, in this study, submesoscale (SBM) fronts (see Thomas et al., 2008). The fronts are the result of advective stirring of buoyancy anomalies by mesoscale eddies (50–200 km in size). SBM fronts are now recognized to be one of the major contributors to vertical heat fluxes in the oceans and, as such, may modulate the global ocean heat budget and therefore the Earth's climate (Balwada et al., 2021; Richards et al., 2021; Siegelman et al., 2020; Su et al., 2018, 2020; Yu et al., 2019).

Idealized modeling studies, with weak internal wave energy, further emphasize that SBM fronts can evolve over time scales shorter than 1 day, with the resulting SBM frontal dynamics having an impact on vertical heat fluxes as large as SBM fronts with longer time scales (Balwada et al., 2021; Gula et al., 2014; Hakim et al., 2002; Lapeyre et al., 2006). A critical issue when assessing these fast-evolving frontal dynamics is that, although internal waves (IGWs) and SBM fronts share similar temporal and spatial scales, each has unique dynamical features (Balwada et al., 2018; Su et al., 2020; Torres et al., 2018). Internal gravity waves, including waves forced by

tidal and near-inertial motions, quickly propagate horizontally (unlike SBM motions) and are associated with large vertical velocities but do not transport heat or other tracers. So far, separating IGWs and SBMs at these short time scales has never been addressed, since most studies remove the IGW contamination using a low-pass filter of one-to-three days, which also removes SBM contributions at short time scales (Qiu et al., 2016, 2020; Su et al., 2020).

Here, we show that it is possible to separate IGWs and SBM frontal dynamics at short time scales and to recover the vital properties of SBM frontal dynamics in terms of intense divergence and vertical velocities. Our approach is based on the analysis of the vertical scales of oceanic motions. This analysis, as well as canonical IGW models (Garret & Munk, 1972), show that energetic IGWs are characterized by having large vertical scales whereas SBMs are characterized by smaller vertical scales. This scale separation is used to effectively separate these two types of motion. The approach of filtering large vertical scales is successfully tested in a simulation of the CCS, a region west of the California coast where IGWs are energetic (Kim et al., 2011; Mazloff et al., 2020). Results indicate that the proposed approach effectively removes the contamination of horizontal and vertical motions by IGWs and yet retains SBM frontal dynamics at time scales shorter than 1 day. The next section presents the CCS numerical simulation, run with 500-m horizontal grid spacing, which will be used to evaluate our approach. The spatial and temporal characteristics of SBMs and IGWs in the CCS, described in Section 3, emphasize the high energy level of IGWs that contaminate SBM fronts. Section 4 details our approach for separating IGWs and SBMs. Section 5 examines the recovered characteristics of SBM frontal dynamics at time scales less than a day and, in particular, their modulation by atmospheric forcings. Discussion and conclusions follow in the last section.

2. Numerical Simulation

The regional CCS simulation considered in this study has been obtained via nesting within the global ocean numerical simulation known as LLC4320, which has a nominal grid spacing of 1/48° (∼2 km at midlatitudes) (Torres et al., 2018). More details on LLC4320 simulation are provided in Flexas et al. (2019) and in the Supporting Information S1. The CCS simulation has horizontal grid spacing of 500 m and 90 vertical levels. As described by Mazloff et al. (2020), the regional CCS simulation was forced by hourly LLC4320 fields at the lateral boundaries, which includes forcing by external and internal tides, near-inertial waves, and higher-frequency IGWS. These lateral boundary conditions produce a realistic IGW spectrum (Mazloff et al., 2020).

The domain considered is the central CCS (Figure 1a), extending from the coast to a longitude of 128°W and spanning the latitudes 35°N to 40°N.

The CCS simulation outputs span 1 December 2011 to 15 May 2012. The present work is focused on the period from April 1–20, 2012. Model outputs have been compared with observations from a mooring whose location is shown by the red star on Figure 1a — see Supporting Information S1 for a discussion of this comparison.

3. Dynamics in the CCS

3.1. Two Dynamical Regimes

Figure 1a shows a typical SST field in the CCS during spring, displaying warm and cold waters separated by a sharp meandering SST front. The cold region, east of the front, corresponds to upwelling, extending up to 300 km from the coast. This upwelling region exhibits a temperature of ∼11°C and has a thermocline at 155 m depth, as shown on Figure 1d. The warm region west of the front, the offshore region, is characterized by temperatures warmer by ∼3–4°C and a main thermocline at 255 m depth (Figure 1d). The mixed-layer (ML) depth is ∼50 m on both sides of the sharp front. The two regions exhibit different vertical stratification (Figure 1d), with the fluid weakly stratified below the ML down to 200 m in the offshore region ($N/f \sim 15$, with N the Brunt-Väisälä frequency and f the Coriolis frequency) and moderately stratified below the ML down to 100 m ($N/f \sim 50$) in the upwelling region.

Dynamics in the CCS are analyzed by partitioning motions into a rotational part, ζ, and a divergent part, δ (Kundu et al., 1990), with ζ and δ defined as $\zeta = v_x - u_y$, $\delta = u_x + v_y$, where u and v are the horizontal velocity components

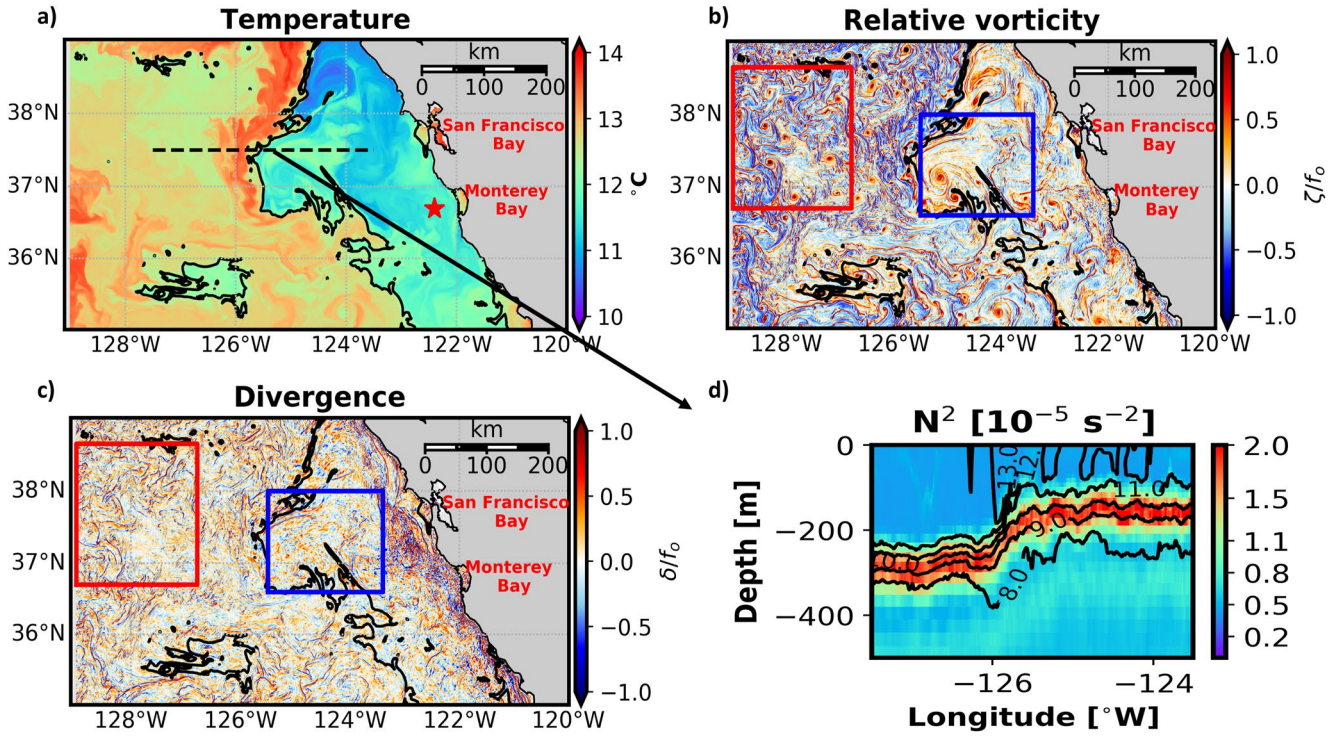

Figure 1. Potential temperature (a), relative vorticity (b), divergence near the surface (c), and vertical section of N^2 (d) in the California Current System. The black isolines in panels a–c show the 12.3°C isotherm. The isotherm close to the coast marks the position of the upwelling front. The contours in (d) are isotherms. The simulated mixed layer depth is ∼50 m in both regions. The blue and red squares correspond, respectively, to the upwelling and offshore regions analyzed in this study. The red star in (a) shows the location of the MBARI-M2 mooring (see Supporting Information S1).

in Cartesian coordinates x and y. The relative vorticity ζ is related to the spin of horizontal motions and the horizontal divergence δ is related to the vertical derivative of the vertical velocity via the 3D incompressibility condition. Both ζ and δ are normalized by f, which corresponds to a period of 19.94 hr in the CCS. Fields of ζ/f and δ/f are shown on, respectively, panels 1b and 1c.

The offshore region, west of the sharp front, includes numerous cyclonic vortices and cyclonic and anticyclonic vorticity filaments with 2–20-km size (Figure 1b). These structures are characterized by ζ/f magnitudes of up to four and therefore have characteristic time scales as small as 5 hr. Cyclonic vortices have larger sizes in the upwelling region and the density of filamentary ζ/f structures is smaller than in the offshore region, although their magnitudes are still large (up to three). These ζ/f structures slowly propagate in both regions, as confirmed by the ζ/f movie in the Supporting Information S1, which is a characteristic of mesoscale eddies and SBMs (Thomas et al., 2008). The δ/f field (Figure 1c) also has large magnitudes (up to three) but its spatial structures significantly differ from the ζ field, in particular in the upwelling region, where it involves incoherent patterns instead of vortices and filaments. The δ/f structures quickly propagate in this region, as displayed by the δ/f movie in the Supporting Information S1, which suggests that they are principally associated with IGWs. Analysis of ζ/f and δ/f fields at different times within 2 months confirms these characteristics.

Examination of Figures 1b and 1c further indicates that ζ/f magnitudes are larger than δ/f magnitudes in the offshore region whereas ζ/f and δ/f magnitudes are similar in the upwelling region. This suggests the existence of two dynamical regimes with IGWs dominating the divergence field in the upwelling region whereas SBMs are more dominant in the offshore region. Differences between these two regions are likely explained in terms of vertical stratification (Siegelman, 2020) but an in-depth study is required to confirm this hypothesis. Nevertheless, these differences emphasize the challenge of separating SBMs from IGWs in the upwelling region. Consequently, the following sections focus on the upwelling region (blue box in Figure 1b) with the results for the offshore region (red box in Figure 1c) shown in the Supporting Information S1.

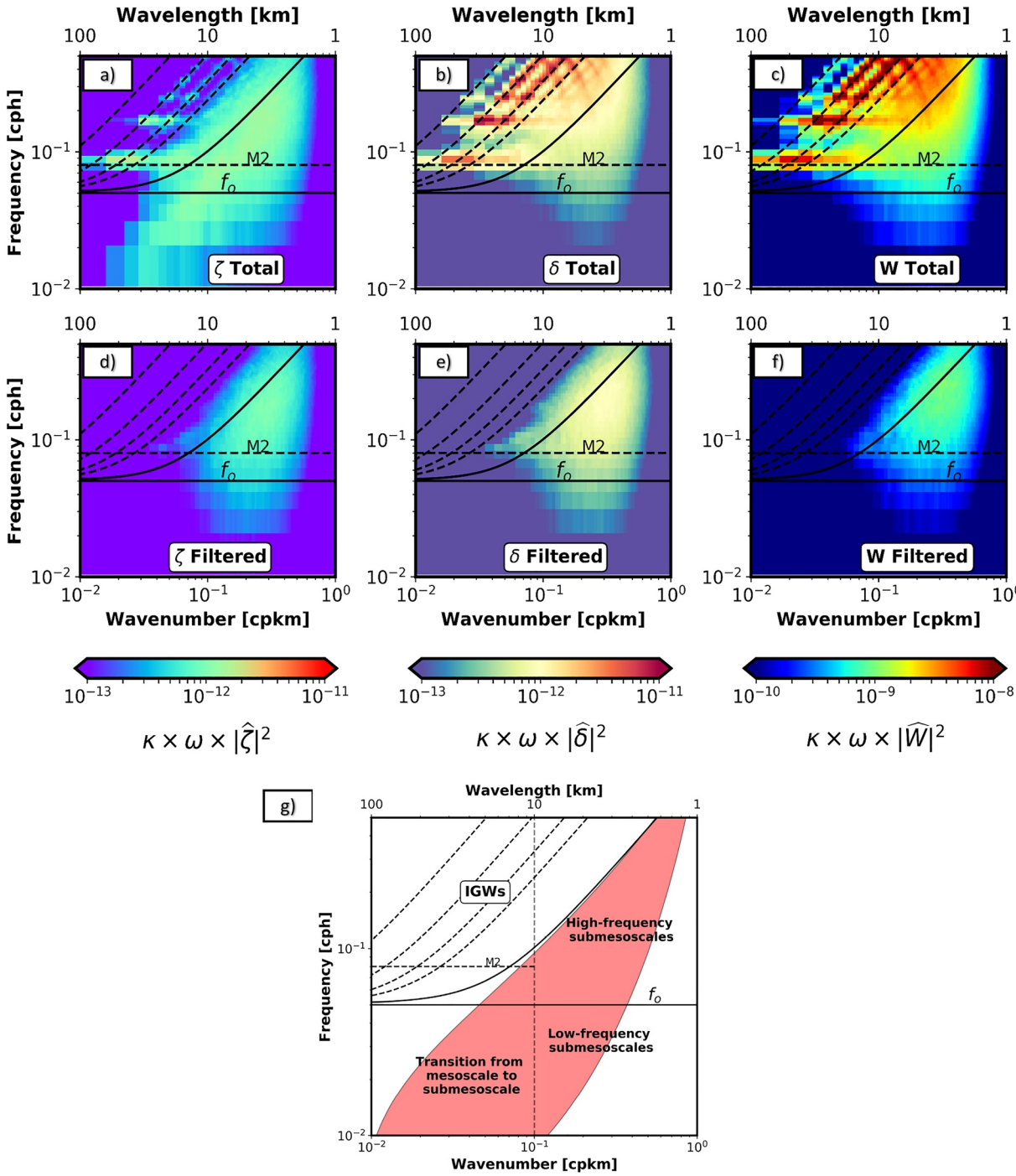

Figure 2. Near-surface spectra of ζ/f (a) and (d), δ/f (b) and (e), and vertical velocity (c) and (f). Panels (a), (b), and (c) concern the total (unfiltered) fields and panels (d), (e), and (f) the filtered fields. These spectra are presented in variance-preserving form. Panel g is a schematic spectrum indicating the location of different classes of motions, which include the transition from mesoscales to submesoscales and internal gravity waves.

3.2. Relative Vorticity and Divergence in the Upwelling Region

The relative importance of mesoscale eddies, SBMs and IGWs is better revealed when moving to the frequency-wavenumber space, that is, the ω-k spectral space, with ω the frequency and k the isotropic horizontal wavenumber (Balwada et al., 2018; Cao et al., 2019, 2021; Su et al., 2020; Torres et al., 2018). The schematic spectrum of Figure 2g indicates the location of the different classes of motions in the spectral space. They include

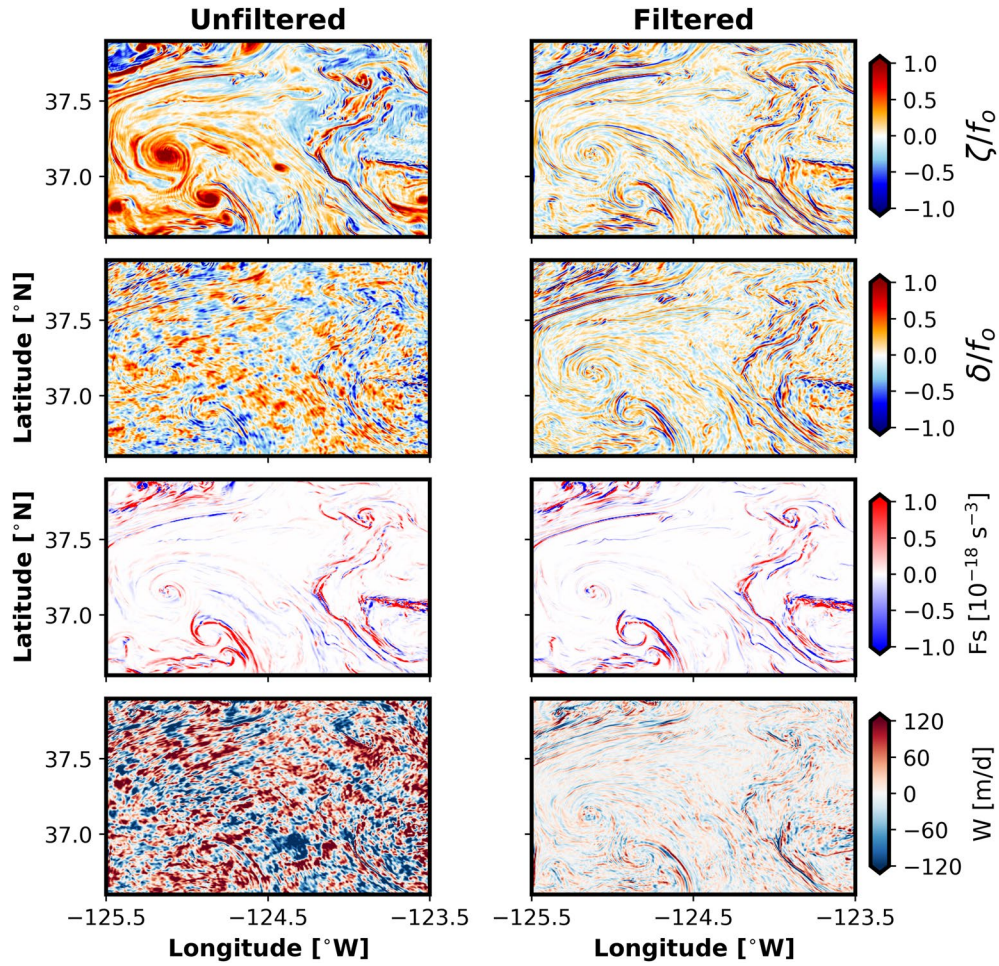

Figure 3. Snapshots in the upwelling region of the total (first column) and filtered (second column) fields of ζ/f (first row), δ/f (second row), F_s (third row), and vertical velocity w at 40 m (last row).

mesoscale eddies, SBMs with low and high frequencies, and IGWs. Additionally, the schematic spectrum shows the IGW linear dispersion relation curves associated with baroclinic modes (dashed lines are for the first five modes and solid line for the tenth mode), which helps to identify energetic IGWs. Mesoscale eddies are usually thought to occupy the spectral domain outside the spectral area where baroclinic modes are plotted, with mesoscale eddies having periods of several days and spatial scales from 20 to 100 km for the blue box in Figure 1b. The SBM spectral domain is assumed in the present study to be outside the spectral area where baroclinic modes are plotted and to comprise scales smaller than 10 km and periods as small as a few hours, as hypothesized in other studies (Cao et al., 2019, 2021; Torres et al., 2018). We refer the reader to Torres et al. (2018) for the methodology used to compute the ω-k spectra.

In the upwelling region, most of the ζ/f variance (Figure 2a) is spread over an area along a sloped line going from 50 km (0.02 cpkm) and 4 days (0.01 cph) to 1 km and 2 hr (0.5 cph). This variance principally arises from mesoscale eddies and SBMs (Capet et al., 2008). The spectral distribution of the δ/f variance (Figure 2b) dramatically differs, with the largest δ/f-variance spread along the first five baroclinic modes, indicating a clear domination of the δ/f field by linear IGWs. These strikingly different spectral characteristics explain the conspicuous discrepancies between the ζ/f and δ/f fields in physical space (Figure 3, first and second rows in the left column). They confirm that the ζ/f field is dominated by mesoscale eddies and SBM filaments whereas the δ/f field is dominated by IGWs. These results illustrate the challenge to meet, since it is impossible from the fields in physical space to recover the divergence properties associated with SBM frontal dynamics. The situation is not so dramatic in the offshore region (not shown): most of the ζ/f and δ/f variance in spectral space are found in the areas explained by

mesoscale eddies and SBMs, with the ζ/f variance larger in the mesoscale eddy area. This is consistent with the ζ/f and δ/f fields in physical space (see Figure S8 in Supporting Information S1).

4. A Dynamical Filter to Separate IGWs and SBMs

From the preceding spectral analysis, IGW variance is captured by low baroclinic modes. Inspection of the dispersion relation curves associated with these modes (dashed lines on Figure 2) indicates that IGWs can have both large horizontal scales with frequencies close to f and also small horizontal scales with shorter time scales. Thus, IGWs share the same small horizontal length scales and time scales as SBMs. However, the definition of baroclinic vertical normal modes is such that low modes are characterized by large vertical scales and high modes by small vertical scales (see section S2 in Supporting Information S1). These vertical scales are identified by the zero-crossing of the vertical profiles of baroclinic modes (Fu & Flierl, 1980; Hua & Haidvogel, 1986). In the upwelling region, the first 10 baroclinic modes do not display any zero-crossing within the moderately-stratified layer above the more stratified thermocline (see Figure S2 in Supporting Information S1). We further assume that SBMs are trapped within the layer above the main thermocline, since they usually emerge only in weakly or moderately stratified layers (Fox-Kemper et al., 2008; Siegelman, 2020; Thomas et al., 2008), and therefore have vertical scales smaller than the thermocline depth.

To separate IGWs and SBMs, we propose application of a high-pass filter to the vertical scales above the thermocline. To do so, we use least squares to fit a line to the velocity profile between the surface and a fixed depth near the thermocline — 80 m for the upwelling region and 200 m for the offshore region. Choosing different depths (110 m for the upwelling region and 220 m for the offshore region) did not change the results. This linear fit is assumed to capture low-mode IGW contributions. The fields before removal of this low-mode contribution are hereinafter referred to as unfiltered and the fields after removal of this contribution (see Figure S2 in Supporting Information S1) are referred to as filtered and indicated by a tilde, for example, $\tilde{\zeta}$.

Although the unfiltered ζ/f, δ/f, and vertical velocity (w) fields differ (Figure 3, first, second, and fourth row in left column), the filtered $\tilde{\zeta}/f$, $\tilde{\delta}/f$, and $\tilde{w}$ fields (Figure 3, first, second, and fourth row in right column) look strikingly similar, displaying positive and negative elongated filaments with magnitudes of order one for ζ/f and δ/f. Movies of the ζ/f, δ/f, and w fields before and after filtering (see Supporting Information S1) emphasize that, although the original quantities quickly propagate because of the IGWs, the filtered quantities are very slowly propagating. To further test whether these filtered fields are associated with SBM frontal dynamics, we have estimated the frontogenesis tendency, F_s (Hoskins & Bretherton, 1972; Lapeyre et al., 2006), which refers to the tendency of buoyancy gradients, embedded in a mesoscale strain field, to increase or decrease (see section S3.1 in Supporting Information S1). Thus F_s indicates whether SBM fronts experience frontogenesis ($F_s > 0$) or frontolysis ($F_s < 0$) (see Supporting Information S1). Figure 3 (third row) shows that F_s fields before and after applying the dynamical filter have the same elongated patterns, indicating that IGWs have almost no impact on F_s. However, whereas the unfiltered ζ/f, δ/f, and w fields differ significantly from the F_s-field, the three filtered fields are similar to F_s (Figure 3), confirming that the filtered patterns of $\tilde{\zeta}/f$, $\tilde{\delta}/f$, and $\tilde{w}$ are closely associated with SBM frontal dynamics.

Comparison of ζ/f, δ/f, and w spectra before and after dynamical filtering (see Figure 2) confirms that the dynamical filter removes the IGW variance captured by the low baroclinic modes. Furthermore, the contribution from mesoscale eddies, in particular to the ζ/f field, is also removed by the dynamical filter (Figure 2a and 2d), which is consistent when comparing fields on the first row of Figure 3. One explanation is that mesoscale eddies typically have an aspect ratio between horizontal and vertical scales close to N/f and therefore are associated with large vertical scales. Comparison of the unfiltered and filtered ζ/f, δ/f, and w fields in the offshore region in physical and spectral space (see Figure S8 in Supporting Information S1) reveals similar results, although not as striking since the δ/f and w fields are less dominated by IGWs.

5. Recovering Short Timescale Frontal Properties Using the Dynamical Filter

We now check the phase relationship, at time scales less than a day, between F_s and the unfiltered and filtered quantities, ζ/f, δ/f, and w to further test the efficiency of separating IGWs and SBMs. This relationship is influenced at short time scales when SBM fronts are affected by the diurnal cycle of atmospheric forcings, as

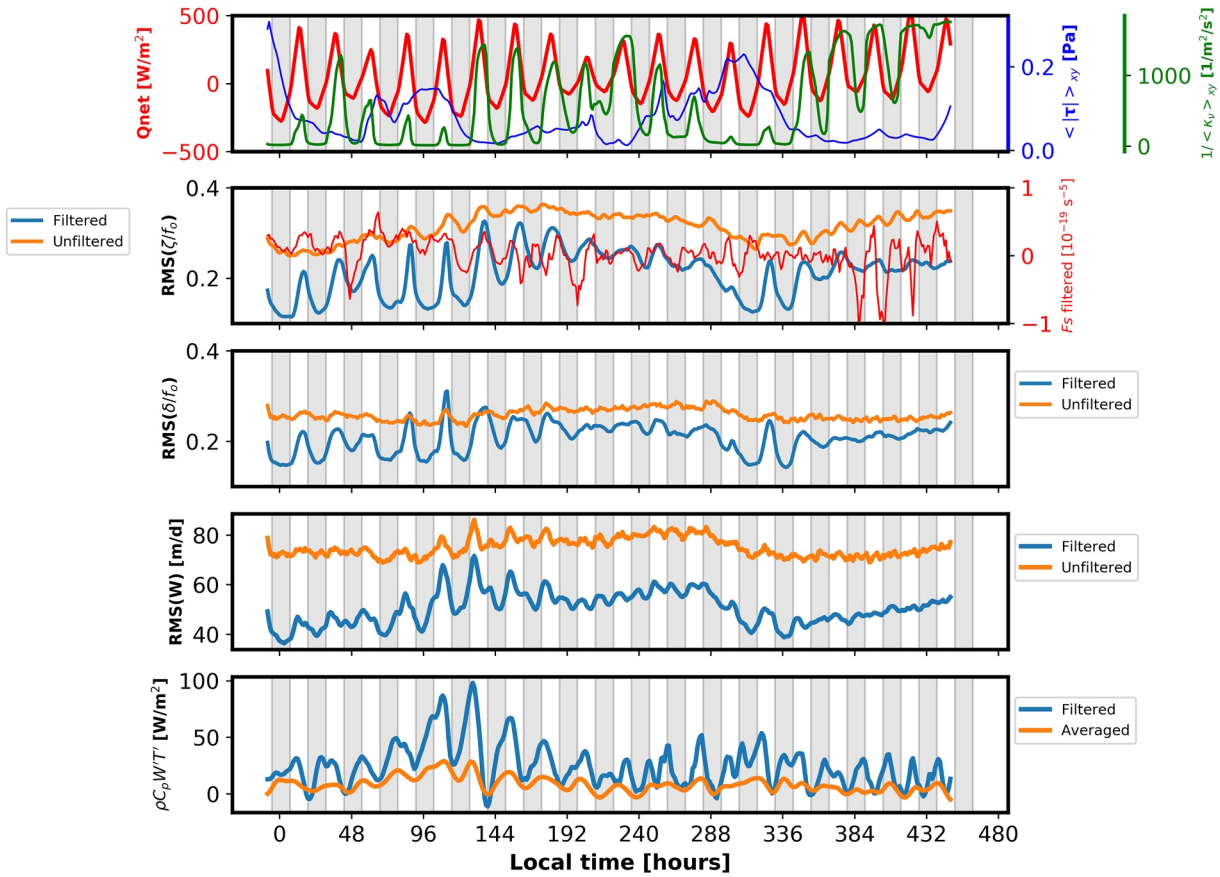

Figure 4. Time evolution in the upwelling region of the net surface heat flux (Q_{net}), wind stress (τ), and ν (top panel), ζ_{rms}/f, and F_s filtered (second panel), δ_{rms}/f (third panel), w_{rms} (fourth panel), and vertical heat fluxes ($\rho C_p W'T'$, bottom panel). RMS values have been calculated over the blue-square region displayed in Figure 1. Other quantities are the mean values calculated over the same region. $1/\nu$ is plotted instead of ν to better emphasize the relationship between Q_{net} and ν as well as with other variables. Orange (blue) curves in panels 2–4 correspond to rms-values before (after) applying the dynamical filter. Blue (orange) curve in the bottom panel corresponds to the vertical heat fluxes after applying the dynamical filter (before applying the dynamical filter and after applying a 1-day low-pass filter) to T and w. The gray shading on each panel shows day time (white) and night time (gray).

emphasized by studies in regions of very weak IGW activity (Peng et al., 2021; Sun et al., 2020). To proceed, we analyze the time series of F_s and RMS values of the unfiltered and filtered quantities over 20 days. We include the time series of vertical viscosity (ν) in the upper oceanic layers since atmospheric forcings are known to impact the frontal dynamics through the vertical viscosity (Garrett & Loder, 1981; Gula et al., 2014) (see also section S5 in the Supporting Information S1).

The time series of the air-sea heat fluxes (Q_{net}, red curve on the top panel of Figure 4), as well as that of the vertical viscosity (ν, green curve on the same panel), show that there is a strong phase relationship between Q_{net} and ν, with ν small during the day because of heating ($Q_{net} > 0$) and ν increasing at night because of cooling ($Q_{net} < 0$). The frontogenesis tendency, F_s, exhibits a clear relationship with atmospheric forcing, with frontogenesis ($F_s > 0$) statistically emphasized during the day and frontolysis ($F_s < 0$) during the night.

The time series of the unfiltered ζ_{rms}/f, δ_{rms}/f, and w_{rms} (orange curves on Figure 4) do not exhibit any significant relationship with atmospheric forcings and F_s. However, time series of the filtered quantities, $\tilde{\zeta}_{rms}/f$, $\tilde{\delta}_{rms}/f$, and $\tilde{w}_{rms}$ (blue curves on Figure 4), exhibit a clear relationship with atmospheric forcings and F_s. During the day (white vertical bands on Figure 4), frontogenesis ($F_s > 0$) is associated with large magnitudes of filtered $\tilde{\zeta}_{rms}/f$, $\tilde{\delta}_{rms}/f$, and $\tilde{w}_{rms}$. During the night (gray vertical bands on Figure 4) when $F_s < 0$, magnitudes of these filtered quantities are smaller. Such phase relationship at short time scales between F_s and filtered quantities is consistent with theoretical and experimental studies (Dauhajre et al., 2017; Peng et al., 2021; Sun et al., 2020). Filtered $\tilde{\zeta}_{rms}/f$ time series have, on average, a smaller magnitude than the total field since contributions from mesoscale eddies are removed by the filter. Similarly, filtered $\tilde{\delta}_{rms}/f$ and $\tilde{w}_{rms}$ time series have a smaller magnitude than the

unfiltered δ_{rms}/f and w_{rms} time series, confirming that IGWs significantly obscure divergence and vertical velocity associated with SBM fronts. These results emphasize the efficiency of the dynamical filter for separating IGWs and SBMs and its ability to recover SBM frontal dynamics at short time scales. Similar results have been obtained in the offshore region (see Figure S9 in Supporting Information S1).

Efficiency of the dynamical filter is further highlighted by the comparison between the vertical heat fluxes using the filtered temperature (T) and w, and those obtained by using T and w averaged over 1 day to remove IGWs (blue and orange curves in bottom panel of Figure 4). Magnitudes of the former are at least two times larger than magnitudes of the latter.

6. Discussion and Conclusions

Recovering SBM frontal dynamics in the presence of high IGW activity is a critical issue for diagnosing the vertical transport of heat, nutrients and important climatic gases in the global ocean. Using low-pass temporal filters to remove IGW contributions, as employed in several studies (Qiu et al., 2016, 2020), also removes the high-frequency part of SBM frontal dynamics. A spatial filter that removes large horizontal scales results in an incomplete removal of IGWs, as illustrated in the Supporting Information S1. The challenge is that IGWs and SBM fronts share the same ranges of short time scales and small horizontal scales.

To address this issue, the present study relies on two assumptions. First, energetic IGWs are assumed to be captured by low baroclinic modes and therefore by vertical scales larger than the thickness of the weakly or moderately-stratified layer above the more stratified thermocline. Second, SBMs are assumed to be trapped within this weakly or moderately-stratified layer and therefore captured by smaller vertical scales. These two assumptions open up the possibility to remove the contamination of oceanic SBMs by IGWs. Our results confirm that filtering the contribution of large vertical scales to the 3-D velocity fields, here operationally carried out by removing a linear fit above the thermocline, leads to an almost complete recovery of SBM frontal dynamics at short time scales, in particular, for relative vorticity, divergence, and vertical velocity fields. This separation permits diagnosis of strong, frontally-induced vertical velocities at short time scales and their impact on vertical heat fluxes.

The assumptions considered in this study do not exclude the possibility that IGWs can interact with SBM fronts, as suggested by several studies (e.g., Thomas, 2017). These studies highlight the importance of accurately capturing wave-wave interactions that transfer energy from large scales to small scales, leading to high-frequency IGWs that may interact with SBM fronts. The realism of the CCS MITgcm configuration used in this study needs to be further tested using a simulation with higher spatial resolution and non-hydrostatic physics. Field experiments dedicated to SBMs usually do not capture such wave-wave interactions because of the spatial and temporal resolutions of the observations (Dove et al., 2021; Siegelman et al., 2020; Thompson et al., 2016). However, observations from the ongoing Sub-Mesoscale Ocean Dynamics Experiment (S-MODE) CCS campaigns should have the appropriate resolution to capture these interactions and, consequently, to evaluate the methodology developed in our study.

Data Availability Statement

The MBARI-M2 mooring data were collected and made freely available (http://dods.mbari.org/data/ssdsdata/deployments/m2/) by the Monterrey Bay Aquarium Research Institute. High-end computing resources were provided by the NASA Advanced Supercomputer (NAS) Division at the Ames Research Center. Model output from global 1/48° MITgcm simulation (known as LLC4320) is freely available online (https://data.nas.nasa.gov/ecco/data.php?dir=/eccodata/llc_4320). Model data analyzed in this paper are also freely available online (https://data.nas.nasa.gov/smode/smodedata/data/scenario_1/).

References

Balwada, D., Smith, K. S., & Abernathey, R. (2018). Submesoscale vertical velocities enhance tracer subduction in an idealized Antarctic Circumpolar Current. *Geophysical Research Letters*, *45*(18), 9790–9802. https://doi.org/10.1029/2018gl079244

Balwada, D., Xiao, Q., Smith, S., Abernathey, R., & Gray, A. (2021). Vertical fluxes conditioned on vorticity and strain reveal submesoscale ventilation. *Journal of Physical Oceanography*. https://doi.org/10.1175/jpo-d-21-0016.1

Acknowledgments
This work was performed at the Jet Propulsion Laboratory, California Institute of Technology under prime contract with NASA (80NM0018D0004), and was awarded under NASA Research Announcement (NRA) NNH17ZDA001N-EVS3, Research Opportunities in Space and Earth Science (ROSES-2017), Appendix A.34: Earth Venture Suborbital-3; NASA Sub-Mesoscale Ocean Dynamics Experiment (NASA S-MODE). Copyright 2021 California Institute of Technology. US government sponsorship acknowledged. P. Klein acknowledges support from the SWOT Science Team, the NASA S-Mode project and the QuickSCat mission. E. D'Asaro was supported by NASA Award Number, 80NSSC19K1007. A. F. Thompson was supported by the NASA S-MODE project and PDRDF funding from NASA's Jet Propulsion Laboratory. L. Siegelman acknowledges the generous support of the Scripps Institutional Postdoctoral Program. D. Menemenlis was supported by S-MODE and by the NASA Physical Oceanography (PO) and Modeling, Analysis, and Prediction (MAP) programs. High-end computing were provided by the NASA Advanced Supercomputing (NAS) Division at the Ames Research Center. This study has been much inspired and motivated by the S-MODE project and the DopplerScatt instrument. H. S. Torres. ran the high-resolution CCS simulation. H. S. Torres and P.Klein led the data analysis and data interpretation and drafted the manuscript. The main original idea of this study was proposed by E. D'Asaro. All authors contributed to the scientific interpretation of the results and reviewed the manuscript. We thank Shane Keating and the other anonymous reviewer for their insightful comments and suggestions that helped to clarify our results.

Cao, H., Fox-Kemper, B., & Jing, Z. (2021). Submesoscale eddies in the upper ocean of the Kuroshio Extension from high-resolution simulation: Energy budget. *Journal of Physical Oceanography*, *51*(7), 2181–2201. https://doi.org/10.1175/jpo-d-20-0267.1

Cao, H., Jing, Z., Fox-Kemper, B., Yan, T., & Qi, Y. (2019). Scale transition from geostrophic motions to internal waves in the northern South China Sea. *Journal of Geophysical Research: Oceans*, *124*(12), 9364–9383. https://doi.org/10.1029/2019jc015575

Capet, X., McWilliams, J. C., Molemaker, M. J., & Shchepetkin, A. F. (2008). Mesoscale to submesoscale transition in the California Current System. Part I: Flow structure, eddy flux, and observational tests. *Journal of Physical Oceanography*, *38*(1), 29–43. https://doi.org/10.1175/2007jpo3671.1

D'Asaro, E., Lee, C., Rainville, L., Harcourt, R., & Thomas, L. (2011). Enhanced turbulence and energy dissipation at ocean fronts. *Science*, *332*(6027), 318–322.

Dauhajre, D. P., McWilliams, J. C., & Uchiyama, Y. (2017). Submesoscale coherent structures on the continental shelf. *Journal of Physical Oceanography*, *47*, 2949–2976. https://doi.org/10.1175/JPO-D-16-0270.1

Dove, L. A., Thompson, A. F., Balwada, D., & Gray, A. R. (2021). Observational evidence of ventilation hotspots in the Southern Ocean. *Journal of Geophysical Research: Oceans*, e2021JC017178. https://doi.org/10.1029/2021jc017178

Ferrari, R. (2011). A frontal challenge for climate models. *Science*, *332*(6027), 316–317. https://doi.org/10.1126/science.1203632

Flexas, M. M., Thompson, A. F., Torres, H. S., Klein, P., Farrar, J. T., Zhang, H., & Menemenlis, D. (2019). Global estimates of the energy transfer from the wind to the ocean, with emphasis on near-inertial oscillations. *Journal of Geophysical Research: Oceans*, *124*(8), 5723–5746. https://doi.org/10.1029/2018jc014453

Fox-Kemper, B., Danabasoglu, G., Ferrari, R., Griffies, S., Hallberg, R., Holland, M., et al. (2011). Parameterization of mixed layer eddies. III: Implementation and impact in global ocean climate simulations. *Ocean Modelling*, *39*(1–2), 61–78. https://doi.org/10.1016/j.ocemod.2010.09.002

Fox-Kemper, B., Ferrari, R., & Hallberg, R. (2008). Parameterization of mixed layer eddies. Part I: Theory and diagnosis. *Journal of Physical Oceanography*, *38*(6), 1145–1165. https://doi.org/10.1175/2007jpo3792.1

Fu, L.-L., & Flierl, G. R. (1980). Nonlinear energy and enstrophy transfers in a realistically stratified ocean. *Dynamics of Atmospheres and Oceans*, *4*(4), 219–246. https://doi.org/10.1016/0377-0265(80)90029-9

Garrett, C. J. R., & Loder, J. (1981). Dynamical aspects of shallow sea fronts. *Philosophical Transactions of the Royal Society of London - Series A: Mathematical and Physical Sciences*, *302*(1472), 563–581.

Garrett, C. J. R., & Munk, C. (1972). Space-time scales of internal waves. *Geophysical Fluid Dynamics*, *3*(3), 225–264. https://doi.org/10.1080/03091927208236082

Gula, J., Molemaker, M. J., & McWilliams, J. C. (2014). Submesoscale cold filaments in the Gulf Stream. *Journal of Physical Oceanography*, *44*(10), 2617–2643. https://doi.org/10.1175/jpo-d-14-0029.1

Hakim, G. J., Snyder, C., & Muraki, D. J. (2002). A new surface model for cyclone–Anticyclone asymmetry. *Journal of the Atmospheric Sciences*, *59*(16), 2405–2420. https://doi.org/10.1175/1520-0469(2002)059<2405:ansmfc>2.0.co;2

Hoskins, B. J., & Bretherton, F. P. (1972). Atmospheric frontogenesis models: Mathematical formulation and solution. *Journal of the Atmospheric Sciences*, *29*(1), 11–37. https://doi.org/10.1175/1520-0469(1972)029<0011:afmmfa>2.0.co;2

Hua, B. L., & Haidvogel, D. B. (1986). Numerical simulations of the vertical structure of quasi-geostrophic turbulence. *Journal of the Atmospheric Sciences*, *43*(23), 2923–2936. https://doi.org/10.1175/1520-0469(1986)043<2923:nsotvs>2.0.co;2

Kim, S. Y., Terrill, E. J., Cornuelle, B. D., Jones, B., Washburn, L., Moline, M. A., & Crawford, G. (2011). Mapping the US West Coast surface circulation: A multiyear analysis of high-frequency radar observations. *Journal of Geophysical Research*, *116*(C3). https://doi.org/10.1029/2010jc006669

Klein, P., Lapeyre, G., Siegelman, L., Qiu, B., Fu, L.-L., Torres, H., et al. (2019). Ocean-scale interactions from space. *Earth and Space Science*.

Kundu, P. K., Cohen, I. M., & Dowling, D. R. (1990). *Fluid mechanics*. Academic press.

Lapeyre, G., Klein, P., & Hua, B. L. (2006). Oceanic restratification forced by surface frontogenesis. *Journal of Physical Oceanography*, *36*(8), 1577–1590. https://doi.org/10.1175/jpo2923.1

Mazloff, M. R., Cornuelle, B., Gille, S. T., & Wang, J. (2020). The importance of remote forcing for regional modeling of internal waves. *Journal of Geophysical Research: Oceans*, *125*(2), e2019JC015623. https://doi.org/10.1029/2019jc015623

Peng, J.-P., Umlauf, L., Dräger-Dietel, J., & North, R. P. (2021). Diurnal variability of frontal dynamics, instability, and turbulence in a submesoscale upwelling filament. *Journal of Physical Oceanography*. https://doi.org/10.1175/jpo-d-21-0033.1

Qiu, B., Chen, S., Klein, P., Torres, H., Wang, J., Fu, L.-L., & Menemenlis, D. (2020). Reconstructing upper-ocean vertical velocity field from sea surface height in the presence of unbalanced motion. *Journal of Physical Oceanography*, *50*(1), 55–79. https://doi.org/10.1175/jpo-d-19-0172.1

Qiu, B., Chen, S., Klein, P., Ubelmann, C., Fu, L.-L., & Sasaki, H. (2016). Reconstructability of three-dimensional upper-ocean circulation from SWOT sea surface height measurements. *Journal of Physical Oceanography*, *46*(3), 947–963. https://doi.org/10.1175/jpo-d-15-0188.1

Richards, K. J., Whitt, D. B., Brett, G., Bryan, F. O., Feloy, K., & Long, M. C. (2021). The impact of climate change on ocean submesoscale activity. *Journal of Geophysical Research: Oceans*, *126*(5), e2020JC016750. https://doi.org/10.1029/2020jc016750

Siegelman, L. (2020). Energetic submesoscale dynamics in the ocean interior. *Journal of Physical Oceanography*, *50*(3), 727–749. https://doi.org/10.1175/jpo-d-19-0253.1

Siegelman, L., Klein, P., Rivière, P., Thompson, A. F., Torres, H. S., Flexas, M., & Menemenlis, D. (2020). Enhanced upward heat transport at deep submesoscale ocean fronts. *Nature Geoscience*, *13*(1), 50–55. https://doi.org/10.1038/s41561-019-0489-1

Su, Z., Torres, H., Klein, P., Thompson, A. F., Siegelman, L., Wang, J., et al. (2020). High-frequency submesoscale motions enhance the upward vertical heat transport in the global ocean. *Journal of Geophysical Research: Oceans*, *125*(9), e2020JC016544. https://doi.org/10.1029/2020jc016544

Su, Z., Wang, J., Klein, P., Thompson, A. F., & Menemenlis, D. (2018). Ocean submesoscales as a key component of the global heat budget. *Nature Communications*, *9*(1), 775. https://doi.org/10.1038/s41467-018-02983-w

Sun, D., Bracco, A., Barkan, R., Berta, M., Dauhajre, D., Molemaker, M. J., et al. (2020). Diurnal cycling of submesoscale dynamics: Lagrangian implications in drifter observations and model simulations of the northern gulf of Mexico. *Journal of Physical Oceanography*, *50*(6), 1605–1623. https://doi.org/10.1175/jpo-d-19-0241.1

Thomas, L. N. (2017). On the modifications of near-inertial waves at fronts: Implications for energy transfer across scales. *Ocean Dynamics*, *67*(10), 1335–1350.

Thomas, L. N., Tandon, A., & Mahadevan, A. (2008). Submesoscale processes and dynamics. *Ocean modeling in an Eddying Regime*, *177*, 17–38. https://doi.org/10.1029/177gm04

Thompson, A. F., Lazar, A., Buckingham, C., Naveira Garabato, A. C., Damerell, G. M., & Heywood, K. J. (2016). Open-ocean submesoscale motions: A full seasonal cycle of mixed layer instabilities from gliders. *Journal of Physical Oceanography*, *46*(4), 1285–1307. https://doi.org/10.1175/jpo-d-15-0170.1

Torres, H. S., Klein, P., Menemenlis, D., Qiu, B., Su, Z., Wang, J., et al. (2018). Partitioning ocean motions into balanced motions and internal gravity waves: A modeling study in anticipation of future space missions. *Journal of Geophysical Research: Oceans*, *123*(11), 8084–8105. https://doi.org/10.1029/2018jc014438

Yu, X., Naveira Garabato, A. C., Martin, A. P., Buckingham, C. E., Brannigan, L., & Su, Z. (2019). An annual cycle of submesoscale vertical flow and restratification in the upper ocean. *Journal of Physical Oceanography*, *49*(6), 1439–1461. https://doi.org/10.1175/jpo-d-18-0253.1